

DESY-03-041

March 2003

A search for resonance decays to lepton+jet at HERA and limits on leptoquarks

ZEUS Collaboration

Abstract

A search for narrow-width resonances that decay into electron+jet or neutrino+jet has been performed with the ZEUS detector at HERA operating at center-of-mass energies of 300 and 318 GeV. An integrated e^+p luminosity of 114.8 pb⁻¹ and e^-p luminosity of 16.7 pb⁻¹ were used. No evidence for any resonance was found. Limits were derived on the Yukawa coupling, λ , as a function of the mass of a hypothetical resonance that has arbitrary decay branching ratios into eq or νq . These limits also apply to squarks predicted by R -parity-violating supersymmetry. Limits for the production of leptoquarks described by the Buchmüller-Rückl-Wyler model were also derived for masses up to 400 GeV. For $\lambda = 0.1$, leptoquark masses up to 290 GeV are excluded.

The ZEUS Collaboration

S. Chekanov, M. Derrick, D. Krakauer, J.H. Loizides¹, S. Magill, B. Musgrave, J. Repond,
R. Yoshida

Argonne National Laboratory, Argonne, Illinois 60439-4815ⁿ

M.C.K. Mattingly

Andrews University, Berrien Springs, Michigan 49104-0380

P. Antonioli, G. Bari, M. Basile, L. Bellagamba, D. Boscherini, A. Bruni, G. Bruni,
G. Cara Romeo, L. Cifarelli, F. Cindolo, A. Contin, M. Corradi, S. De Pasquale, P. Giusti,
G. Iacobucci, A. Margotti, R. Nania, F. Palmonari, A. Pesci, G. Sartorelli, A. Zichichi
University and INFN Bologna, Bologna, Italy^e

G. Aghuzumtsyan, D. Bartsch, I. Brock, S. Goers, H. Hartmann, E. Hilger, P. Irrgang,
H.-P. Jakob, A. Kappes², U.F. Katz², O. Kind, U. Meyer, E. Paul³, J. Rautenberg,
R. Renner, H. Schnurbusch⁴, A. Stifutkin, J. Tandler, K.C. Voss, M. Wang, A. Weber⁵
Physikalisches Institut der Universität Bonn, Bonn, Germany^b

D.S. Bailey⁶, N.H. Brook⁶, J.E. Cole, B. Foster, G.P. Heath, H.F. Heath, S. Robins,
E. Rodrigues⁷, J. Scott, R.J. Tapper, M. Wing
H.H. Wills Physics Laboratory, University of Bristol, Bristol, United Kingdom^m

M. Capua, A. Mastroberardino, M. Schioppa, G. Susinno
Calabria University, Physics Department and INFN, Cosenza, Italy^e

J.Y. Kim, Y.K. Kim, J.H. Lee, I.T. Lim, M.Y. Pac⁸
Chonnam National University, Kwangju, Korea⁹

A. Caldwell⁹, M. Helbich, X. Liu, B. Mellado, Y. Ning, S. Paganis, Z. Ren, W.B. Schmidke,
F. Sciulli
Nevis Laboratories, Columbia University, Irvington on Hudson, New York 10027^o

J. Chwastowski, A. Eskreys, J. Figiel, K. Olkiewicz, P. Stopa, L. Zawiejski
Institute of Nuclear Physics, Cracow, Polandⁱ

L. Adamczyk, T. Bóld, I. Grabowska-Bóld, D. Kisiielewska, A.M. Kowal, M. Kowal,
T. Kowalski, M. Przybycień, L. Suszycki, D. Szuba, J. Szuba¹⁰
*Faculty of Physics and Nuclear Techniques, University of Mining and Metallurgy, Cracow,
Poland^p*

A. Kotański¹¹, W. Słomiński¹²
Department of Physics, Jagellonian University, Cracow, Poland

V. Adler, L.A.T. Bauerdick¹³, U. Behrens, I. Bloch, K. Borrás, V. Chiochia, D. Dannheim, G. Drews, J. Fourletova, U. Fricke, A. Geiser, F. Goebel⁹, P. Göttlicher¹⁴, O. Gutsche, T. Haas, W. Hain, G.F. Hartner, S. Hillert, B. Kahle, U. Kötz, H. Kowalski¹⁵, G. Kramberger, H. Labes, D. Lelas, B. Löhr, R. Mankel, I.-A. Melzer-Pellmann, M. Moritz¹⁶, C.N. Nguyen, D. Notz, M.C. Petrucci¹⁷, A. Polini, A. Raval, U. Schneekloth, F. Selonke³, H. Wessoleck, G. Wolf, C. Youngman, W. Zeuner

Deutsches Elektronen-Synchrotron DESY, Hamburg, Germany

S. Schlenstedt

DESY Zeuthen, Zeuthen, Germany

G. Barbagli, E. Gallo, C. Genta, P. G. Pelfer

University and INFN, Florence, Italy^e

A. Bamberger, A. Benen, N. Coppola

Fakultät für Physik der Universität Freiburg i.Br., Freiburg i.Br., Germany^b

M. Bell, P.J. Bussey, A.T. Doyle, C. Glasman, J. Hamilton, S. Hanlon, S.W. Lee, A. Lupi, D.H. Saxon, I.O. Skillicorn

Department of Physics and Astronomy, University of Glasgow, Glasgow, United Kingdom^m

I. Gialas

Department of Engineering in Management and Finance, Univ. of Aegean, Greece

B. Bodmann, T. Carli, U. Holm, K. Klimek, N. Krumnack, E. Lohrmann, M. Milite, H. Salehi, S. Stonjek¹⁸, K. Wick, A. Ziegler, Ar. Ziegler

Hamburg University, Institute of Exp. Physics, Hamburg, Germany^b

C. Collins-Tooth, C. Foudas, R. Gonçalo⁷, K.R. Long, A.D. Tapper

Imperial College London, High Energy Nuclear Physics Group, London, United Kingdom^m

P. Cloth, D. Filges

Forschungszentrum Jülich, Institut für Kernphysik, Jülich, Germany

M. Kuze, K. Nagano, K. Tokushuku¹⁹, S. Yamada, Y. Yamazaki

Institute of Particle and Nuclear Studies, KEK, Tsukuba, Japan^f

A.N. Barakbaev, E.G. Boos, N.S. Pokrovskiy, B.O. Zhautykov

Institute of Physics and Technology of Ministry of Education and Science of Kazakhstan, Almaty, Kazakhstan

H. Lim, D. Son

Kyungpook National University, Taegu, Korea^g

K. Piotrkowski

Institut de Physique Nucléaire, Université Catholique de Louvain, Louvain-la-Neuve, Belgium

F. Barreiro, O. González, L. Labarga, J. del Peso, E. Tassi, J. Terrón, M. Vázquez
Departamento de Física Teórica, Universidad Autónoma de Madrid, Madrid, Spain^l

M. Barbi, F. Corriveau, S. Gliga, J. Lainesse, S. Padhi, D.G. Stairs
Department of Physics, McGill University, Montréal, Québec, Canada H3A 2T8^a

T. Tsurugai
Meiji Gakuin University, Faculty of General Education, Yokohama, Japan

A. Antonov, P. Danilov, B.A. Dolgoshein, D. Gladkov, V. Sosnovtsev, S. Suchkov
Moscow Engineering Physics Institute, Moscow, Russia^j

R.K. Dementiev, P.F. Ermolov, Yu.A. Golubkov, I.I. Katkov, L.A. Khein, I.A. Korzhavina, V.A. Kuzmin, B.B. Levchenko²⁰, O.Yu. Lukina, A.S. Proskuryakov, L.M. Shcheglova, N.N. Vlasov, S.A. Zotkin
Moscow State University, Institute of Nuclear Physics, Moscow, Russia^k

N. Coppola, S. Grijpink, E. Koffeman, P. Kooijman, E. Maddox, A. Pellegrino, S. Schagen, H. Tiecke, J.J. Velthuis, L. Wiggers, E. de Wolf
NIKHEF and University of Amsterdam, Amsterdam, Netherlands^h

N. Brümmner, B. Bylsma, L.S. Durkin, T.Y. Ling
*Physics Department, Ohio State University, Columbus, Ohio 43210*ⁿ

A.M. Cooper-Sarkar, A. Cottrell, R.C.E. Devenish, J. Ferrando, G. Grzelak, S. Patel, M.R. Sutton, R. Walczak
Department of Physics, University of Oxford, Oxford United Kingdom^m

A. Bertolin, R. Brugnera, R. Carlin, F. Dal Corso, S. Dusini, A. Garfagnini, S. Limentani, A. Longhin, A. Parenti, M. Posocco, L. Stanco, M. Turcato
Dipartimento di Fisica dell'Università and INFN, Padova, Italy^e

E.A. Heaphy, F. Metlica, B.Y. Oh, J.J. Whitmore²¹
Department of Physics, Pennsylvania State University, University Park, Pennsylvania 16802^o

Y. Iga
Polytechnic University, Sagami-hara, Japan^f

G. D'Agostini, G. Marini, A. Nigro
Dipartimento di Fisica, Università 'La Sapienza' and INFN, Rome, Italy^e

C. Cormack²², J.C. Hart, N.A. McCubbin
Rutherford Appleton Laboratory, Chilton, Didcot, Oxon, United Kingdom^m

C. Heusch
*University of California, Santa Cruz, California 95064*ⁿ

I.H. Park
Department of Physics, Ewha Womans University, Seoul, Korea

N. Pavel
Fachbereich Physik der Universität-Gesamthochschule Siegen, Germany

H. Abramowicz, A. Gabareen, S. Kananov, A. Kreisel, A. Levy
Raymond and Beverly Sackler Faculty of Exact Sciences, School of Physics, Tel-Aviv University, Tel-Aviv, Israel^d

T. Abe, T. Fusayasu, S. Kagawa, T. Kohno, T. Tawara, T. Yamashita
Department of Physics, University of Tokyo, Tokyo, Japan^f

R. Hamatsu, T. Hirose³, M. Inuzuka, S. Kitamura²³, K. Matsuzawa, T. Nishimura
Tokyo Metropolitan University, Department of Physics, Tokyo, Japan^f

M. Arneodo²⁴, M.I. Ferrero, V. Monaco, M. Ruspa, R. Sacchi, A. Solano
Università di Torino, Dipartimento di Fisica Sperimentale and INFN, Torino, Italy^e

T. Koop, G.M. Levman, J.F. Martin, A. Mirea
Department of Physics, University of Toronto, Toronto, Ontario, Canada M5S 1A7^a

J.M. Butterworth, C. Gwenlan, R. Hall-Wilton, T.W. Jones, M.S. Lightwood, B.J. West
Physics and Astronomy Department, University College London, London, United Kingdom^m

J. Ciborowski²⁵, R. Ciesielski²⁶, R.J. Nowak, J.M. Pawlak, J. Sztuk²⁷, T. Tymieniecka²⁸,
A. Ukleja²⁸, J. Ukleja, A.F. Żarnecki
Warsaw University, Institute of Experimental Physics, Warsaw, Poland^g

M. Adamus, P. Plucinski
Institute for Nuclear Studies, Warsaw, Poland^g

Y. Eisenberg, L.K. Gladilin²⁹, D. Hochman, U. Karshon
Department of Particle Physics, Weizmann Institute, Rehovot, Israel^c

D. Kçira, S. Lammers, L. Li, D.D. Reeder, A.A. Savin, W.H. Smith
*Department of Physics, University of Wisconsin, Madison, Wisconsin 53706*ⁿ

A. Deshpande, S. Dhawan, V.W. Hughes, P.B. Straub
*Department of Physics, Yale University, New Haven, Connecticut 06520-8121*ⁿ

S. Bhadra, C.D. Catterall, S. Fourletov, G. Hartner, S. Menary, M. Soares, J. Standage
Department of Physics, York University, Ontario, Canada M3J 1P3^a

- ¹ also affiliated with University College London
- ² on leave of absence at University of Erlangen-Nürnberg, Germany
- ³ retired
- ⁴ now at Sparkasse Koeln
- ⁵ self-employed
- ⁶ PPARC Advanced fellow
- ⁷ supported by the Portuguese Foundation for Science and Technology (FCT)
- ⁸ now at Dongshin University, Naju, Korea
- ⁹ now at Max-Planck-Institut für Physik, München/Germany
- ¹⁰ partly supported by the Israel Science Foundation and the Israel Ministry of Science
- ¹¹ supported by the Polish State Committee for Scientific Research, grant no. 2 P03B 09322
- ¹² member of Dept. of Computer Science
- ¹³ now at Fermilab, Batavia/IL, USA
- ¹⁴ now at DESY group FEB
- ¹⁵ on leave of absence at Columbia Univ., Nevis Labs., N.Y./USA
- ¹⁶ now at CERN
- ¹⁷ now at INFN Perugia, Perugia, Italy
- ¹⁸ now at Univ. of Oxford, Oxford/UK
- ¹⁹ also at University of Tokyo
- ²⁰ partly supported by the Russian Foundation for Basic Research, grant 02-02-81023
- ²¹ on leave of absence at The National Science Foundation, Arlington, VA/USA
- ²² now at Univ. of London, Queen Mary College, London, UK
- ²³ present address: Tokyo Metropolitan University of Health Sciences, Tokyo 116-8551, Japan
- ²⁴ also at Università del Piemonte Orientale, Novara, Italy
- ²⁵ also at Łódź University, Poland
- ²⁶ supported by the Polish State Committee for Scientific Research, grant no. 2 P03B 07222
- ²⁷ Łódź University, Poland
- ²⁸ supported by German Federal Ministry for Education and Research (BMBF), POL 01/043
- ²⁹ on leave from MSU, partly supported by University of Wisconsin via the U.S.-Israel BSF

- ^a supported by the Natural Sciences and Engineering Research Council of Canada (NSERC)
- ^b supported by the German Federal Ministry for Education and Research (BMBF), under contract numbers HZ1GUA 2, HZ1GUB 0, HZ1PDA 5, HZ1VFA 5
- ^c supported by the MINERVA Gesellschaft für Forschung GmbH, the Israel Science Foundation, the U.S.-Israel Binational Science Foundation and the Benozio Center for High Energy Physics
- ^d supported by the German-Israeli Foundation and the Israel Science Foundation
- ^e supported by the Italian National Institute for Nuclear Physics (INFN)
- ^f supported by the Japanese Ministry of Education, Science and Culture (the Monbusho) and its grants for Scientific Research
- ^g supported by the Korean Ministry of Education and Korea Science and Engineering Foundation
- ^h supported by the Netherlands Foundation for Research on Matter (FOM)
- ⁱ supported by the Polish State Committee for Scientific Research, grant no. 620/E-77/SPUB-M/DESY/P-03/DZ 247/2000-2002
- ^j partially supported by the German Federal Ministry for Education and Research (BMBF)
- ^k supported by the Fund for Fundamental Research of Russian Ministry for Science and Education and by the German Federal Ministry for Education and Research (BMBF)
- ^l supported by the Spanish Ministry of Education and Science through funds provided by CICYT
- ^m supported by the Particle Physics and Astronomy Research Council, UK
- ⁿ supported by the US Department of Energy
- ^o supported by the US National Science Foundation
- ^p supported by the Polish State Committee for Scientific Research, grant no. 112/E-356/SPUB-M/DESY/P-03/DZ 301/2000-2002, 2 P03B 13922
- ^q supported by the Polish State Committee for Scientific Research, grant no. 115/E-343/SPUB-M/DESY/P-03/DZ 121/2001-2002, 2 P03B 07022

1 Introduction

Many extensions of the Standard Model (SM) predict the existence of particles carrying both baryon and lepton numbers, such as leptoquarks (LQs) [1] or squarks (in R -parity-violating (\mathcal{R}_p) supersymmetry) [2]. In ep collisions at HERA, such states may be produced directly through electron¹-quark fusion, with subsequent decay into electron and quark or neutrino and quark, yielding peaks in the spectra of the final-state lepton-jet invariant mass, M_{lj} . This paper presents a search for such resonant states.

The only significant backgrounds to high-mass resonance production arise from neutral current (NC) and charged current (CC) deep inelastic scattering (DIS), as illustrated in Figs. 1a and b. While a resonance with mass below the HERA center-of-mass energy, \sqrt{s} , would give rise to narrow peak in the M_{lj} spectrum, the backgrounds from NC and CC fall rapidly at high mass due to the dependence of the cross section on Q^2 , the virtuality of the exchanged bosons, and to the sharply falling valence-quark density at large Bjorken x . The variable θ^* , the lepton scattering angle in the lepton-jet center-of-mass frame, can be used to reduce the DIS backgrounds. The decay of a resonance results in an angular distribution different from those produced by SM processes: a scalar resonance, for example, will have a flat distribution in $\cos \theta^*$, while NC DIS events follow approximately a $1/(1 - \cos \theta^*)^2$ distribution.

The data were used to investigate the production of resonances. In the absence of a narrow resonance signal, limits can be set on the production of resonances with masses below \sqrt{s} and with the assumption of narrow width, as shown in Fig. 1c. In addition, specific limits on the production of Buchmüller-Rückl-Wyler (BRW) LQs [1] with masses both below and above \sqrt{s} can be obtained. Because backgrounds fall sharply at large M_{lj} , the data are sensitive to LQs via exchange terms, shown in Fig. 1d, as well as interference terms with SM processes. The narrow-width assumption is not necessary for setting limits in the BRW model.

The present results supersede previous analyses [3,4]. They are based on all data collected by the ZEUS experiment in the period from 1994 to 2000. After 1998, the HERA center-of-mass energy was increased from 300 to 318 GeV.

2 Experimental conditions

The ZEUS detector is described in detail elsewhere [5]. The main components used in the present analysis are the central tracking detector (CTD) and the uranium-scintillator

¹ Unless otherwise specified, ‘electron’ refers to both positron and electron and ‘neutrino’ refers to both neutrino and antineutrino.

sampling calorimeter (CAL).

Charged particles are tracked in the CTD [6], which operates in a magnetic field of 1.43 T provided by a thin superconducting solenoid. The CTD consists of 72 cylindrical drift chamber layers, organized in nine superlayers covering the polar-angle region $15^\circ < \theta < 164^\circ$. The transverse-momentum resolution for full-length tracks is $\sigma(p_T)/p_T = 0.0058p_T \oplus 0.0065 \oplus 0.0014/p_T$, with p_T in GeV.

The CAL [7] consists of three parts: the forward² (FCAL), the barrel (BCAL) and the rear (RCAL) calorimeters. Each part is divided into modules, which are subdivided transversely into towers and longitudinally into one electromagnetic section (EMC) and either one (in RCAL) or two (in BCAL and FCAL) hadronic sections (HAC). The smallest subdivision of the calorimeter is called a cell. The CAL energy resolutions, as measured under test-beam conditions, are $\sigma(E)/E = 0.18/\sqrt{E}$ for electrons and $\sigma(E)/E = 0.35/\sqrt{E}$ for hadrons, with E in GeV. The timing resolution of the CAL is better than 1 ns for energy deposits greater than 4.5 GeV. Further performance parameters of the CAL relevant for this study have been discussed in previous publications [3, 4].

The forward plug calorimeter (FPC), a lead-scintillator sandwich calorimeter, was installed in the 20×20 cm² beam hole of the forward CAL (FCAL) of the ZEUS detector in 1998. Although the FPC information was not used in this analysis, the impact of its material on the CAL response to forward jets was extensively studied.

The luminosity, which was measured [8] from the rate of the bremsstrahlung process $ep \rightarrow ep\gamma$, has an uncertainty of 1.6% to 2.25%, depending on the running periods. All ZEUS data collected from 1994 to 2000 are listed in Table 1, and were used for this analysis.

3 Monte Carlo simulation

Production and decay of resonances were simulated using PYTHIA 6.1 [9, 10], which takes into account the finite width of the resonant state, but includes only the s -channel diagrams. Initial- and final-state QCD radiation from the quark and the effect of LQ hadronization [10] before decay as well as the initial-state QED radiation from the electron are also taken into account.

Standard Model NC and CC DIS events were simulated using the HERACLES 4.6.2 [11] program with the DJANGO 6 version 2.4 [12] and DJANGOH 1.1 [13] interfaces to

² The ZEUS coordinate system is a right-handed Cartesian system, with the Z axis pointing in the proton beam direction, referred to as the “forward direction”, and the X axis pointing left towards the center of HERA. The coordinate origin is at the nominal interaction point.

the hadronization programs. Radiative corrections for initial- and final-state electroweak radiations, vertex and propagator corrections, and two-boson exchange were included. The hadronic final state was simulated using the MEPS model in LEPTO 6.5 [14], which includes $O(\alpha_S)$ matrix elements and higher-order QCD radiation. The CTEQ5D parton distribution function (PDF) [15] was used in evaluating the SM cross sections.

The largest uncertainty in the NC and CC cross sections is due to the uncertainties in the parton densities of the proton. The PDFs at high Bjorken x are determined primarily from measurements made in fixed-target DIS experiments. At $x = 0.6$, corresponding to a lepton-jet mass of 230 GeV, the cross-section uncertainty due to the PDF uncertainty [16] is $\approx 6\%$ for NC and ≈ 4 (10)% for e^-u (e^+d) CC reactions, where u and d refer to the u and d valence quarks, respectively.

The generated events were passed through the GEANT 3.13-based [17] ZEUS detector- and trigger-simulation programs [5]. They were reconstructed and analysed by the same program chain as the data.

4 Resonance search

Events from a hypothetical resonance decaying into eq (νq) have a topology identical to DIS NC (CC) events. Events originating from high-mass resonances are expected to have high transverse energy, at least one jet, and either an identified final-state electron or large missing transverse energy. The lepton-jet invariant mass was calculated as

$$M_{lj} = \sqrt{2E_l E_j (1 - \cos \xi)},$$

where E_l is the energy of the outgoing lepton, E_j is the energy of the jet, and ξ is the angle between the lepton and jet. In final states containing multiple jets, the jet with the largest transverse momentum, P_T^j , was used.

4.1 $ep \rightarrow eX$ topology

4.1.1 Event selection

Events with the topology $ep \rightarrow eX$, where X contains one or more jets, were selected using the following criteria:

- the Z coordinate of the reconstructed event vertex was required to be in the range $|Z| < 50$ cm, consistent with an ep collision;

- the total transverse energy, E_T , was required to be at least 60 GeV. This removes the bulk of the SM NC background;
- an identified electron [18] was required with energy $E'_e > 25$ GeV located either in FCAL or BCAL, corresponding to an electron polar angle, $\theta_e < 126^\circ$. Electrons impacting the BCAL within 1.5 cm of a module edge, as well as electrons impacting between the FCAL and the BCAL, as determined by tracking information, were discarded to ensure that the resolutions were well understood;
- at least one hadronic jet with transverse momentum $P_T^j > 15$ GeV, obtained using the longitudinally invariant k_T cluster algorithm [19] in inclusive mode [20], was required. The centroid at the FCAL face of the highest- P_T jet was required to be outside a box of 60×60 cm² centered on the proton beam, in order to ensure good energy containment and to reduce the systematic uncertainties due to the proton remnant.

The acceptance, mass shifts, and resolutions for resonant lepton-quark states were calculated from the LQ MC. After these cuts, the acceptance for scalar resonances was $\sim 60\%$, depending weakly on the mass. The acceptance for vector resonances was $\sim 60\%$ below 200 GeV, decreasing to $\sim 40\%$ at 290 GeV. These differences in the acceptances for scalar and vector resonances are due to the different decay angular distributions. The mass resolution, determined from a Gaussian fit to the peak of the reconstructed mass spectrum, fell from 6% to 4% as the resonant mass increased from 150 to 290 GeV. The peak position was typically lower than the generated mass by 1%. The resolution in $\cos \theta^*$ near $|\cos \theta^*| = 1$ had a Gaussian width of 0.01, degrading to 0.03 with decreasing $|\cos \theta^*|$.

4.1.2 Search results

After the above selection, 21 509 events were found, compared to $21\,445 \pm 1\,288$ expected from the NC MC simulation and the evaluation of its systematic uncertainties (see Section 4.1.3). The measured distributions of the total transverse energy, E_T , are compared to the simulation in Figs. 2a and 2e, where the e^+p and e^-p samples are shown separately. Also shown are $E - P_Z$ (Figs. 2b,f), where the E and P_Z are summed over the final-state electron and all the hadrons, electron transverse momentum (P_T^e) (Figs. 2c,g) and jet transverse momentum (P_T^j) (Figs. 2d,h). Good agreement is seen between the data and the SM NC simulation for all of these spectra.

Figures 3 and 4 show the M_{ej} spectra for e^+p and e^-p data, respectively. The upper plots show the spectra with and without the cut $\cos \theta^* < 0.4$, while the lower plots show the ratio of the observed spectrum to SM expectations with no $\cos \theta^*$ cut. The data are well described by the NC MC.

An excess of data events relative to SM expectations was seen in data from the 1994-97 period [3]. For $M_{ej} > 210$ GeV, 24.7 events were expected and 49 were observed. No such excess is seen in the more recent data. The increase in the proton beam energy from 820 to 920 GeV in 1998 had no significant effect on the mass reconstruction or the signal acceptance. The effect of the addition of the FPC was studied extensively; uncertainties in its simulation were found not to affect the conclusions of the present analysis. Combining all the e^+p data, 104 events were observed with $M_{ej} > 210$ GeV, in good agreement with the SM expectation of 90 ± 15 . The systematic uncertainty on the expectation is discussed in the next section. The excess seen in the earlier data sample must be ascribed to a statistical fluctuation.

4.1.3 Systematic uncertainties

The uncertainty on the expected number of events from NC DIS process was investigated. The dominant sources were uncertainties in:

- calorimeter energy scale, of 1% for BCAL electrons, 2% for FCAL electrons and 2% for hadrons. This led to an uncertainty of 4 (12)% in the NC expectation for $M_{ej}=100$ (220) GeV;
- the simulation of the hadronic energy flow including simulation of the proton remnant and the energy flow between the struck quark and proton remnant. Tests based on the SM MC samples yielded variations of the NC background of about 10% for masses above 220 GeV;
- the energy response of FCAL towers closest to the beam from the differences observed between data and simulation. Tests based on the SM MC samples showed variations of the NC background of less than 5% for $M_{ej}=220$ GeV;
- the parton densities, as estimated by Botje [16], which gave an uncertainty of 5% for $M_{ej}=220$ GeV.

Other uncertainties were investigated and found to be small compared to the above items. They are the simulation of the electron-energy resolution, the electron-finding efficiency, the jet-position reconstruction, the luminosity determination and the simulation of the vertex distribution. The overall systematic uncertainties on the background expectations result from summing the contributions from all these sources in quadrature and are shown in Figs. 3b and 4b as the shaded bands.

4.1.4 Significance analysis

To quantify the level of agreement of the M_{ej} spectra between the SM MC and the data, a significance analysis was performed using a sliding mass window of width $3\sigma(M_{ej})$, where $\sigma(M_{ej})$ is the mass resolution discussed in Section 4.1.1. The number of events, μ , expected from the SM and the number of observed events, N , were compared in each window, and the probability of observing N or more events while expecting μ was calculated as

$$P = \sum_{k=N}^{\infty} e^{-\mu} \frac{\mu^k}{k!}. \quad (1)$$

In the e^+p data sample, a minimum probability, P_{min} , of 2.6×10^{-3} was found at mass 121 GeV, where 2575 events were observed while 2436 were expected inside the sliding window. A large number of MC experiments were then performed, taking into account the systematic uncertainties on the SM expectations, and the P_{min} distribution was determined. In 35% of all simulated experiments, the value of P_{min} obtained was less than that found in the data. With the additional cut $\cos\theta^* < 0.4$ applied to the sample, a P_{min} of 1.9×10^{-2} was found in the e^+p data sample at a mass of 158 GeV. A value of P_{min} less than that found in the data was observed in 41% of the generated experiments. The same test was also done on the e^-p data samples. The results are summarized in Table 2. These observations show that the data are compatible with the SM expectation, and there is no evidence for a narrow resonance in the eq channel.

4.2 $ep \rightarrow \nu X$ topology

4.2.1 Event selection

Events with the topology $ep \rightarrow \nu X$, where X contains one or more jets, were selected by the following cuts, similar to those used in the CC cross-section measurement [21]:

- the Z coordinate of the reconstructed event vertex was required to be in the range $|Z| < 50$ cm. The event vertex was reconstructed either using the tracks measured in the CTD (for events with large γ_0 [21], the hadronic scattering angle of the system relative to the nominal interaction point) or from the arrival time of the particles entering the FCAL (for events with small γ_0 , i.e. outside the CTD acceptance);
- the missing transverse momentum, $\cancel{P}_T > 20$ GeV, as measured in the calorimeter;
- $y < 0.9$, where y was calculated from the longitudinal momentum measured in the calorimeter: $y = (E - P_Z)/2E_e$, where $E_e = 27.5$ GeV is the electron beam energy. This cut discards events in which the kinematic variables were poorly reconstructed;

- NC events were removed by discarding events with identified electrons;
- at least one jet was required with $P_T^j > 10$ GeV, where jets were reconstructed as in the $ep \rightarrow eX$ topology, and the centroid at the FCAL face of the highest- P_T jet was required to be outside a box of 60×60 cm² centered on the proton beam.

The neutrino energy and angle were calculated by assuming that \cancel{P}_T and missing $E - P_Z$ were carried away by a single neutrino. Monte Carlo simulations of resonant-state production indicated that the neutrino energy, E_ν , and polar angle, θ_ν , were measured with average resolutions of 16% and 11%, respectively. The average systematic shift in E_ν was less than 2%, while the shift in θ_ν was less than 1%. After all these cuts, the acceptance was $\sim 60\%$, depending weakly on the mass.

The invariant mass of the ν -jet system, $M_{\nu j}$, was reconstructed using the sum of the 4-momenta of the neutrino and the highest- P_T jet in the event. The shift and resolution of the invariant mass were studied by reconstructing it for the LQ MC events and fitting the mass peak with a Gaussian function. The resulting mass shift was below 1% for LQ masses between 150 and 290 GeV, with the resolution varying from 8% to 7%.

4.2.2 Search results

After the selection, 2536 events were found, compared to 2587 ± 217 expected from the CC MC simulation and the evaluation of its systematic uncertainties (see Section 4.2.3). The distributions of \cancel{P}_T are compared for data and simulation in Figs. 5a and 5e, where the e^+p and e^-p samples are shown separately. Also shown are $E - P_Z$ (Figs. 5b,f), where the E and P_Z are summed over the final-state hadrons, E_ν (Figs. 5c,g) and P_T^j (Figs. 5d,h). Reasonable agreement is seen between the data and the SM CC simulation for all of these spectra. A small excess compared to MC is observed for the e^+p data at large \cancel{P}_T (also reflected in the P_T^j and E_ν distributions).

Figures 6 and 7 show the $M_{\nu j}$ spectra for e^+p and e^-p data, respectively. The upper plots show the spectra with and without a cut of $\cos\theta^* < 0.4$, while the lower plots show the ratio of the observed spectra to SM expectations with no $\cos\theta^*$ cut. The data are reasonably well described by the CC MC.

4.2.3 Systematic uncertainties

The uncertainty on the predicted background from SM CC DIS processes was investigated. The dominant sources of uncertainty, which are similar to those described in Section 4.1.3 for the $ep \rightarrow eX$ case, arise from uncertainties in:

- the hadronic energy scale, of 2%, which leads to an uncertainty of 2 (10)% for $M_{\nu j}=100$ (220) GeV;
- the simulation of the energy deposited in the FCAL regions closest to the forward beam pipe, which leads to an uncertainty of $\sim 7\%$ for $M_{\nu j}=220$ GeV;
- the parton densities, as estimated by Botje [16], giving 9% and 4% uncertainties for e^+p and e^-p , respectively, for $M_{\nu j}=220$ GeV. The PDF uncertainties were also estimated using the ZEUS NLO fit [22] with similar results.

Other uncertainties include jet-position reconstruction and luminosity determination, which were small compared to those given above. The overall systematic uncertainties on the background expectations were obtained by summing the contributions from all these sources in quadrature, and are shown in Figs. 6b and 7b as the shaded bands.

4.2.4 Significance analysis

The same significance analysis as applied to the M_{e_j} spectra was performed on the $M_{\nu j}$ spectra. The results are summarized in Table 3. The observations are again compatible with the SM expectation, and there is no evidence for a narrow resonance in the νq channel.

5 Limits on the production of resonant states

Since no evidence was found for a narrow resonance in the lepton-jet mass spectra, limits were set on the Yukawa coupling λ and the production cross section of the eight types of resonant states listed in Table 4 with masses below \sqrt{s} . The resonance decay width was assumed to be small, and the s -channel production was assumed to be dominant, so that the resonance exchange and interference contributions were neglected.

The limits were set using a likelihood technique involving the observables M_{ljs} and $\cos\theta^*$. The variable M_{ljs} is the invariant mass of the lepton-jets system and was calculated from:

$$M_{ljs} = \sqrt{2E_e(E + P_Z)_{ljs}} \quad ,$$

where $E_e = 27.5$ GeV is the electron beam energy, $(E + P_Z)_{ljs}$ was determined using the lepton and all jets in the event satisfying $P_T^j > 15$ GeV ($P_T^j > 10$ GeV in $ep \rightarrow \nu X$ channel) and $\eta_j < 3$ [3, 4].

The M_{ljs} method rather than the M_{l_j} method was used in the limit setting because it has better resolution on the reconstructed resonance mass for $LQ \rightarrow eq$ events. Using

the PYTHIA MC described in Section 3, it was found that the resolution on M_{ljs} for the $LQ \rightarrow eq$ events varied from 3% to 2% as the mass varied from 150 to 290 GeV, while that on M_{lj} varied from 6% to 4%. For the $LQ \rightarrow \nu q$ events, M_{ljs} and M_{lj} have similar resolutions. On the other hand, the M_{ljs} method assumes that the final state consists only of the LQ decay products and the proton remnant. It is also affected by the QED initial-state radiation (ISR) of a photon from the incoming electron. Therefore, the M_{lj} method is more general and better suited for a resonance search. This is discussed in more detail elsewhere [3, 4].

In the limit-setting procedure, the width was assumed to be small compared to the detector resolution, so that the narrow-width approximation (NWA) is valid. In the NWA, the total cross section of the production of a single state is described at Born level [1] by

$$\sigma^{NWA} = (J + 1) \frac{\pi}{4s} \lambda^2 q(x_0, M_{eq}^2), \quad (2)$$

where $q(x_0, M_{eq}^2)$ is the initial-state quark (or antiquark) momentum density in the proton evaluated at $x_0 = M_{eq}^2/s$ and virtuality scale M_{eq}^2 , and J is the spin of the state.

The effect of QED ISR on the resonance production cross section was evaluated. It varies from -4% at resonance mass 100 GeV to -25% at mass 300 GeV and depends weakly on the resonance type. This was taken into account when setting the limits on λ . The next-to-leading-order (NLO) QCD corrections, the so-called K -factors, including the vertex loop corrections, gluon radiation from the leptoquark or the quark and other higher-order diagrams, have been evaluated for the scalar resonances [23, 24]. The K -factor varied from 1.17 (1.17) to 1.15 (1.35) for an eu (ed) resonance with mass varying from 100 to 300 GeV. However, no calculation is available for the vector resonances, so for consistency, no NLO QCD correction was applied to either scalar or vector resonance.

For each of the running periods listed in Table 1, the M_{ljs} - $\cos\theta^*$ plane for $150 < M_{ljs} < 320$ GeV was divided into bins, labelled i , for each of the eq and νq data samples. For resonant states with νq decays, both $eq \rightarrow eX$ and $eq \rightarrow \nu X$ samples were used, while for resonant states decaying only to eq , only $eq \rightarrow eX$ samples were used. The upper limit on the coupling strength, λ_{limit} , as a function of M_{eq} , was obtained by solving ³

$$\int_0^{\lambda_{\text{limit}}^2} d\lambda^2 L(M_{eq}, \lambda) = 0.95 \int_0^{\infty} d\lambda^2 L(M_{eq}, \lambda),$$

where L is the product of Poisson probabilities of all $\cos\theta^*$ - M_{ljs} bins convoluted with

³ With the Bayesian prior assumption of a uniform λ^2 distribution.

Gaussian distributions for the main systematic uncertainties. The L was calculated as

$$L = \int_{-\infty}^{\infty} \prod_j d\delta_j \frac{1}{\sqrt{2\pi}} e^{(-\delta_j^2/2)} \prod_i e^{(-\mu'_i) \frac{\mu'_i N_i}{N_i!}},$$

where j denotes the source of systematic uncertainty and δ_j corresponds to the variation of the j^{th} systematic parameter in units of the nominal values quoted in Sections 4.1.3 and 4.2.3. The index i labels the bin in $\cos\theta^*-M_{ljs}$ and N_i gives the number of events observed in that bin. The variable μ'_i , which denotes the expected number of events in bin i after the effect of the systematic variations, was calculated as

$$\mu'_i = \mu_i \prod_j (1 + \sigma_{ij})^{\delta_j},$$

where μ_i , which depends on the M_{eq} and λ , is the number of expected events in bin i with no systematic variation and σ_{ij} gives the fractional variation of μ_i under the nominal shift in the j^{th} systematic parameter. This definition of μ'_i reduces to a linear dependence of μ'_i on each δ_j when δ_j is small while avoiding the possibility of μ'_i becoming negative which would arise if μ'_i was defined as a linear function of the δ_j 's.

Figure 8 shows the λ limits as a function of β_{eq} and $\beta_{\nu q}$, the branching ratios for $LQ \rightarrow eq$ and $LQ \rightarrow \nu q$, respectively, and as a function of the resonance mass. These limits were obtained for the four scalar resonant states listed in Table 4 and for $\lambda = 0.1$ and $\lambda = 0.3$, where the latter ($\lambda \approx \sqrt{4\pi\alpha_{EW}}$) corresponds to the electroweak (EW) coupling. The equivalent plots for vector resonant states are shown in Fig. 9. For the e^+u and e^-d resonances νq decays are forbidden by charge conservation. The e^-u and e^+d resonances can decay to either eq or νq . The $eq+\nu q$ limits, which assume $\beta_{\nu q} + \beta_{eq} = 1$, are largely independent of the branching ratio, and are typically in excess of 285 GeV for the EW coupling. The limits obtained using only the eq (or the νq) data set allow for decay modes other than eq and νq , so the eq and νq limits are applicable to a wider range of physics models than the combined $eq+\nu q$ results. Similar limits have been presented by the H1 collaboration for scalar e^-d and e^-u resonances [25].

For comparison, the limits on scalar resonances reported by the $D\bar{O}$ experiment [26] at the Tevatron are shown in Fig. 8. For a scalar resonant state with $\beta_{eq}=1$, the $D\bar{O}$ and CDF [27] limits are 225 GeV and 213 GeV, respectively, leading to a combined Tevatron limit of 242 GeV [28]. These limits are independent of both coupling and quark flavor, but degrade (in the case of $D\bar{O}$ for example) to 204 GeV (98 GeV) as β_{eq} decreases from 100% to 50% (0%).

The limits presented in Fig. 8 apply to squarks with \mathcal{R}_p couplings to eq . For example, the λ -limit contours on S_{e+d} with the decay $S_{e+d} \rightarrow e^+d$ (the dashed curves in Fig. 8c) apply

to \tilde{u}_j squarks with coupling λ_{1j1} and subsequent decay $\tilde{u}_j \rightarrow e^+d$, where the subscript j indicates the squark generation. The limit curves on S_{e^-u} with decay $S_{e^-u} \rightarrow e^-u$ (the dashed curves in Fig. 8a) and with $S_{e^-u} \rightarrow \nu d$ (the dotted curves in the same plot) apply to \tilde{d}_j squarks with coupling λ_{11j} and subsequent decays $\tilde{d}_j \rightarrow e^-u$ and $\tilde{d}_j \rightarrow \nu d$, respectively. With the e^-u and νd channels combined and with $\beta_{e^-u} = \beta_{\nu d} = 0.5\beta$, the limit for squark \tilde{d}_j on $\lambda_{11j}\sqrt{\beta}$ is 0.1 for mass 276 GeV and 0.3 for mass 295 GeV. In this case, the R_p -conserving decay branching ratio of $\tilde{d}_j \rightarrow \chi_k q_j$ is $1-\beta$, where χ_k is the gaugino.

The limit on the resonant-state production cross section, σ_{limit} , was calculated by using the NWA as shown in Eq. (2) with $\lambda = \lambda_{\text{limit}}$. Figure 10 shows the results for the scalar and vector resonant states. Limits on the calculated production cross section with only eq data samples (assuming $\beta_{eq} = 0.5$), with only νq data samples (assuming $\beta_{\nu q} = 0.5$) and with all the data samples combined (assuming $\beta_{eq} = \beta_{\nu q} = 0.5$) are shown as a function of M_{eq} . Usually the limit becomes stricter after combining the eq and νq data samples.

6 Limits on BRW leptoquark model

The two-dimensional (M_{ijs} - $\cos\theta^*$) likelihood method described above was also used to set limits on the Yukawa coupling, λ , of the BRW LQs. The full LQ cross section was used, including the s -channel and u -channel contributions and interference with DIS. The difference of the limits thus obtained to those obtained by using NWA is negligible below the LQ mass, M_{LQ} , of 280 GeV.

The coupling limits of the 14 BRW LQs listed in Table 5 were calculated as a function of M_{LQ} . The presence of leptoquarks with $M_{LQ} > \sqrt{s}$ would affect the observed mass spectra, particularly at high mass, mainly due to u -channel exchange and the interference effects. Therefore, it is possible to extend the limits beyond \sqrt{s} . Coupling limits were calculated for masses up to 400 GeV.

The combined search in the $LQ \rightarrow eq$ and $LQ \rightarrow \nu q$ topologies, when applicable, produces more stringent limits on leptoquark production. An example is shown in Fig. 11a for the V_0^L LQ produced through e^+d fusion, which decays to e^+d and $\bar{\nu}u$ with equal probability, and for the S_0^L LQ produced through e^-u fusion, which decays to e^-u and νd with equal probability. The limits obtained with only the eq data samples, only the νq data samples and the combined samples are shown for each LQ. If a coupling strength $\lambda = 0.3$ is assumed, the production of an V_0^L LQ is excluded up to a mass of 284 (286) GeV using eq (νq) samples only, while it is excluded up to 386 GeV with the combined samples. For the S_0^L , the mass limit is 298 (301) GeV using eq (νq) samples only and the combined mass limit is 351 GeV.

Also shown in Fig. 11b are the limits on the S_0^L LQ from $D\bar{O}$, OPAL [29] and L3 [30]. The most stringent limits in the high-mass region (above 200 GeV) from the LEP experiments come from an indirect search through the t -channel LQ exchange between the incoming electron and positron.

Figure 12 shows the coupling limits on the scalar and vector BRW LQs with $F = 0$ and $F = 2$, respectively, where $F = 3B + L$ is the fermion number of the LQ and B and L are the baryon and lepton numbers, respectively. The limits on λ_{LQ} at $M_{LQ} = 400$ GeV range from 0.3 to 1.0. In general, present results are significantly better than LEP limits below 300 GeV and comparable above 300 GeV. The H1 collaboration has presented similar limits on $F = 0$ [31] and $F = 2$ [25] LQs. The excluded mass regions for BRW LQs with $\lambda = 0.1$ and with $\lambda = 0.3$ are summarized in Table 6. They range from 248 to 290 GeV for $\lambda = 0.1$ and from 273 to 386 GeV for $\lambda = 0.3$.

7 Conclusions

The total ep data recorded by the ZEUS experiment at HERA were used to search for the presence of a narrow-width resonance decaying into a lepton and a jet, with the final-state lepton being either an electron or a neutrino. The data samples include 16.7 pb^{-1} of e^-p and 114.8 pb^{-1} of e^+p collisions. No evidence was found for resonance production, either in the eq or νq topology. Limits were set on the coupling strength of resonant states that could decay in these topologies using a two-dimensional likelihood analysis. With the combined eq and νq topologies, a scalar e^-u (e^+d) resonant state is excluded up to a mass of 275 (265) GeV for coupling strength $\lambda = 0.1$. The combined limits depend very weakly on the resonance-decay branching ratio. Limits on the coupling strength of Buchmüller-Rückl-Wyler-type leptoquarks with masses up to 400 GeV are also presented. The excluded mass regions depend on BRW LQ type and the coupling. At $\lambda = 0.1$, they range from 248 to 290 GeV, which are the most stringent limits available to date.

Acknowledgements

We thank the DESY Directorate for their strong support and encouragement, and the HERA machine group for their diligent efforts. We are grateful for the support of the DESY computing and network services. The design, construction and installation of the ZEUS detector have been made possible by the ingenuity and effort of many people who are not listed as authors.

References

- [1] W. Buchmüller, R. Rückl and D. Wyler, *Phys. Lett.* **B 191**, 442 (1987). Erratum in *Phys. Lett.* **B 448**, 320 (1999).
- [2] J. Butterworth and H. Dreiner, *Nucl. Phys.* **B 397**, 3 (1993).
- [3] ZEUS Coll., J. Breitweg et al., *Eur. Phys. J.* **C 16**, 253 (2000).
- [4] ZEUS Coll., J. Breitweg et al., *Phys. Rev.* **D 63**, 052002 (2001).
- [5] ZEUS Coll., U. Holm (ed.), *The ZEUS Detector*. Status Report (unpublished), DESY (1993), available on <http://www-zeus.desy.de/bluebook/bluebook.html>.
- [6] N. Harnew et al., *Nucl. Inst. Meth.* **A 279**, 290 (1989);
B. Foster et al., *Nucl. Phys. Proc. Suppl.* **B 32**, 181 (1993);
B. Foster et al., *Nucl. Inst. Meth.* **A 338**, 254 (1994).
- [7] M. Derrick et al., *Nucl. Inst. Meth.* **A 309**, 77 (1991);
A. Andresen et al., *Nucl. Inst. Meth.* **A 309**, 101 (1991);
A. Caldwell et al., *Nucl. Inst. Meth.* **A 321**, 356 (1992);
A. Bernstein et al., *Nucl. Inst. Meth.* **A 336**, 23 (1993).
- [8] J. Andruszków et al., Preprint DESY-92-066, DESY, 1992;
ZEUS Coll., M. Derrick et al., *Z. Phys.* **C 63**, 391 (1994);
J. Andruszków et al., *Acta Phys. Pol.* **B 32**, 2025 (2001).
- [9] T. Sjöstrand, *Comp. Phys. Comm.* **135**, 238 (2001).
- [10] C. Friberg, E. Norrbin and T. Sjöstrand, *Phys. Lett.* **B 403**, 329 (1997).
- [11] A. Kwiatkowski, H. Spiesberger and H.-J. Möhring, *Comp. Phys. Comm.* **69**, 155 (1992).
- [12] K. Charchula, G.A. Schuler and H. Spiesberger, *Comp. Phys. Comm.* **81**, 381 (1994).
- [13] H. Spiesberger, *HERACLES and DJANGO: Event Generation for ep Interactions at HERA Including Radiative Processes*, 1998, available on <http://www.desy.de/~hspiesb/djangoh.html>.
- [14] G. Ingelman, A. Edin and J. Rathsman, *Comp. Phys. Comm.* **101**, 108 (1997).
- [15] H.L. Lai et al., *Phys. Rev.* **D 55**, 1280 (1997).
- [16] M. Botje, *Eur. Phys. J.* **C 14**, 285 (2000).
- [17] R. Brun et al., GEANT3, Technical Report CERN-DD/EE/84-1, CERN, 1987.
- [18] ZEUS Coll., J. Breitweg et al., *Z. Phys.* **C 74**, 207 (1997).
- [19] S. Catani et al., *Nucl. Phys.* **B 406**, 187 (1993).

- [20] S.D. Ellis and D.E. Soper, Phys. Rev. **D 48**, 3160 (1993).
- [21] ZEUS Coll., J. Breitweg et al., Eur. Phys. J. **C 12**, 411 (2000);
ZEUS Coll., S. Chekanov et al., Phys. Lett. **B 539**, 197 (2002).
- [22] ZEUS Coll., S. Chekanov et al., Phys. Rev. **D 67**, 012007 (2003).
- [23] T. Plehn et al., Z. Phys. **C 74**, 611 (1997).
- [24] Z. Kunszt and W.J. Stirling, Z. Phys. **C 75**, 453 (1997).
- [25] H1 Coll., C. Adloff et al., Phys. Lett. **B 523**, 234 (2001).
- [26] DØ Coll., B. Abbott et al., Phys. Rev. Lett. **79**, 4321 (1997);
DØ Coll., B. Abbott et al., Phys. Rev. Lett. **80**, 2051 (1998);
DØ Coll., V.M. Abazov et al., Phys. Rev. **D 64**, 092004 (2001);
DØ Coll., V.M. Abazov et al., Phys. Rev. Lett. **88**, 191801 (2002).
- [27] CDF Coll., F. Abe et al., Phys. Rev. Lett. **79**, 4327 (1997).
- [28] Leptoquark Limits Combination Working Group, C. Grosso-Pilcher, G. Landsberg
and M. Paterno, Preprint hep-ex/9810015.
- [29] OPAL Coll., G. Abbiendi et al., Eur. Phys. J. **C 6**, 1 (1999).
- [30] L3 Coll., M. Acciari et al., Phys. Lett. **B 489**, 81 (2000).
- [31] H1 Coll., C. Adloff et al., Eur. Phys. J. **C 11**, 447 (1999). Erratum in
Eur. Phys. J. **C 14**, 553 (2000).
- [32] A. Djouadi et al., Z. Phys. **C 46**, 679 (1990).

Period	E_p (GeV)	E_e (GeV)	\sqrt{s} (GeV)	e charge	luminosity (pb^{-1})	δ_{lumi}
94-97	820	27.5	300	e^+	48.5	$\pm 1.6\%$
98-99	920	27.5	318	e^-	16.7	$\pm 1.8\%$
99-00	920	27.5	318	e^+	66.3	$\pm 2.25\%$

Table 1: The characteristics of the three data samples used for the present study; δ_{lumi} is the uncertainty of the measured luminosity.

	No $\cos \theta^*$ cut		$\cos \theta^* < 0.4$	
	e^+p	e^-p	e^+p	e^-p
P_{min}	0.26%	0.032%	1.9%	4.3%
M_{ej} (GeV)	121	151	158	151
N_{obs}	2575	305	73	27
μ_{SM}	2436	249	56.4	18.8
F	35%	6%	41%	56%

Table 2: Results of the significance analysis on the M_{ej} spectra: P_{min} is the minimum probability along the M_{ej} spectra, as defined in Eq. (1); N_{obs} is the number of observed events at the corresponding M_{ej} ; μ_{SM} is the expectation from the SM background; F is the fraction of the simulated experiments with the minimum probability $P < P_{min}$.

	No $\cos \theta^*$ cut		$\cos \theta^* < 0.4$	
	e^+p	e^-p	e^+p	e^-p
P_{min}	1.8%	9.9%	1.1%	24.5%
$M_{\nu j}$ (GeV)	246	225	269	217
N_{obs}	10	22	2	9
μ_{SM}	4.5	16.2	0.16	6.8
F	76%	77%	24%	94%

Table 3: Results of the significance analysis on the $M_{\nu j}$ spectra. For details, see the caption to Table 2.

Scalar			Vector		
Resonance	Charge	Decay	Resonance	Charge	Decay
S_{e^+u}	5/3	e^+u	V_{e^+u}	5/3	e^+u
S_{e^+d}	2/3	e^+d	V_{e^+d}	2/3	e^+d
		$\bar{\nu}u$			$\bar{\nu}u$
S_{e^-u}	-1/3	e^-u	V_{e^-u}	-1/3	e^-u
		νd			νd
S_{e^-d}	-4/3	e^-d	V_{e^-d}	-4/3	e^-d

Table 4: *First-generation scalar and vector resonant states that can be produced in $e^\pm p$ scattering. The top half of the table lists color-triplet states with fermion number $F = L + 3B = 0$, while the bottom half lists those with $F = 2$. The left and right sets of columns list scalars and vectors, respectively.*

LQ species	q	Production	Decay	Branching ratio	Coupling
$S_{1/2}^L$	5/3	$e_R^+ u_R$	$e^+ u$	1	λ_L
$S_{1/2}^R$	5/3	$e_L^+ u_L$	$e^+ u$	1	λ_R
	2/3	$e_L^+ d_L$	$e^+ d$	1	$-\lambda_R$
$\tilde{S}_{1/2}^L$	-2/3	$e_R^+ d_R$	$e^+ d$	1	λ_L
V_0^L	2/3	$e_R^+ d_L$	$e^+ d$	1/2	λ_L
			$\bar{\nu}_e u$	1/2	λ_L
V_0^R	2/3	$e_L^+ d_R$	$e^+ d$	1	λ_R
\tilde{V}_0^R	5/3	$e_L^+ u_R$	$e^+ u$	1	λ_R
V_1^L	5/3	$e_R^+ u_L$	$e^+ u$	1	$\sqrt{2}\lambda_L$
	2/3	$e_R^+ d_L$	$e^+ d$	1/2	$-\lambda_L$
			$\bar{\nu}_e u$	1/2	λ_L
S_0^L	-1/3	$e_L^- u_L$	$e^- u$	1/2	λ_L
			$\nu_e d$	1/2	$-\lambda_L$
S_0^R	-1/3	$e_R^- u_R$	$e^- u$	1	λ_R
\tilde{S}_0^R	-4/3	$e_R^- d_R$	$e^- d$	1	λ_R
S_1^L	-1/3	$e_L^- u_L$	$e^- u$	1/2	$-\lambda_L$
			$\nu_e d$	1/2	$-\lambda_L$
	-4/3	$e_L^- d_L$	$e^- d$	1	$-\sqrt{2}\lambda_L$
$V_{1/2}^L$	-4/3	$e_L^- d_R$	$e^- d$	1	λ_L
$V_{1/2}^R$	-4/3	$e_R^- d_L$	$e^- d$	1	λ_R
	-1/3	$e_R^- u_L$	$e^- u$	1	λ_R
$\tilde{V}_{1/2}^L$	-1/3	$e_L^- u_R$	$e^- u$	1	λ_L

Table 5: The $F = 0$ (upper part) and $F = 2$ (lower part) leptoquark species of the Buchmüller-Rückl-Wyler model [1] and the corresponding couplings. Those LQs that couple only to neutrino and quark and therefore could not be produced at HERA are not listed. The LQ species are classified according to their spin (S for scalar and V for vector), their chirality (L or R) and their weak isospin ($0, 1/2, 1$). The leptoquarks \tilde{S} and \tilde{V} differ by two units of hypercharge from S and V , respectively. In addition, the electric charge q of the leptoquarks, the production channel, as well as their allowed decay channels assuming lepton-flavor conservation are displayed. The nomenclature follows the Aachen convention [32].

LQ Type (F=0)	V_0^L	V_0^R	\tilde{V}_0^R	V_1^L	$S_{1/2}^L$	$S_{1/2}^R$	$\tilde{S}_{1/2}^L$
M(GeV)($\lambda=0.1$)	266	268	282	290	282	282	269
M(GeV)($\lambda=0.3$)	386	287	305	367	308	303	286
LQ Type (F=2)	S_0^L	S_0^R	\tilde{S}_0^R	S_1^L	$V_{1/2}^L$	$V_{1/2}^R$	$\tilde{V}_{1/2}^L$
M(GeV)($\lambda=0.1$)	276	273	248	275	248	274	273
M(GeV)($\lambda=0.3$)	351	298	273	300	277	302	313

Table 6: Mass limit of the 14 BRW LQs at $\lambda=0.1$ and 0.3 .

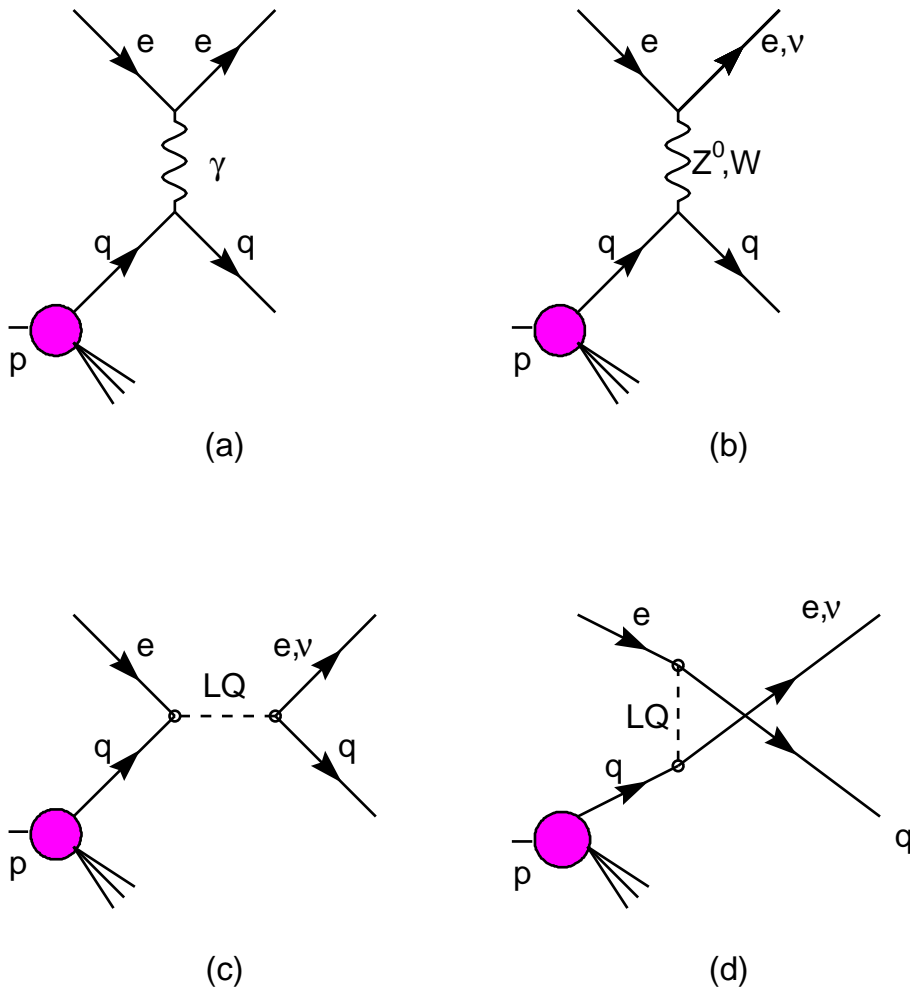


Figure 1: Diagrams for ep scattering at HERA via (a) photon and (b) Z^0 exchange (NC) and via W exchange (CC). The leptoquark diagrams for the same initial and final states are c) s -channel LQ production and d) u -channel LQ exchange. Here e stands for both e^+ (positron) and e^- (electron), and ν for both ν (neutrino) and $\bar{\nu}$ (antineutrino).

ZEUS

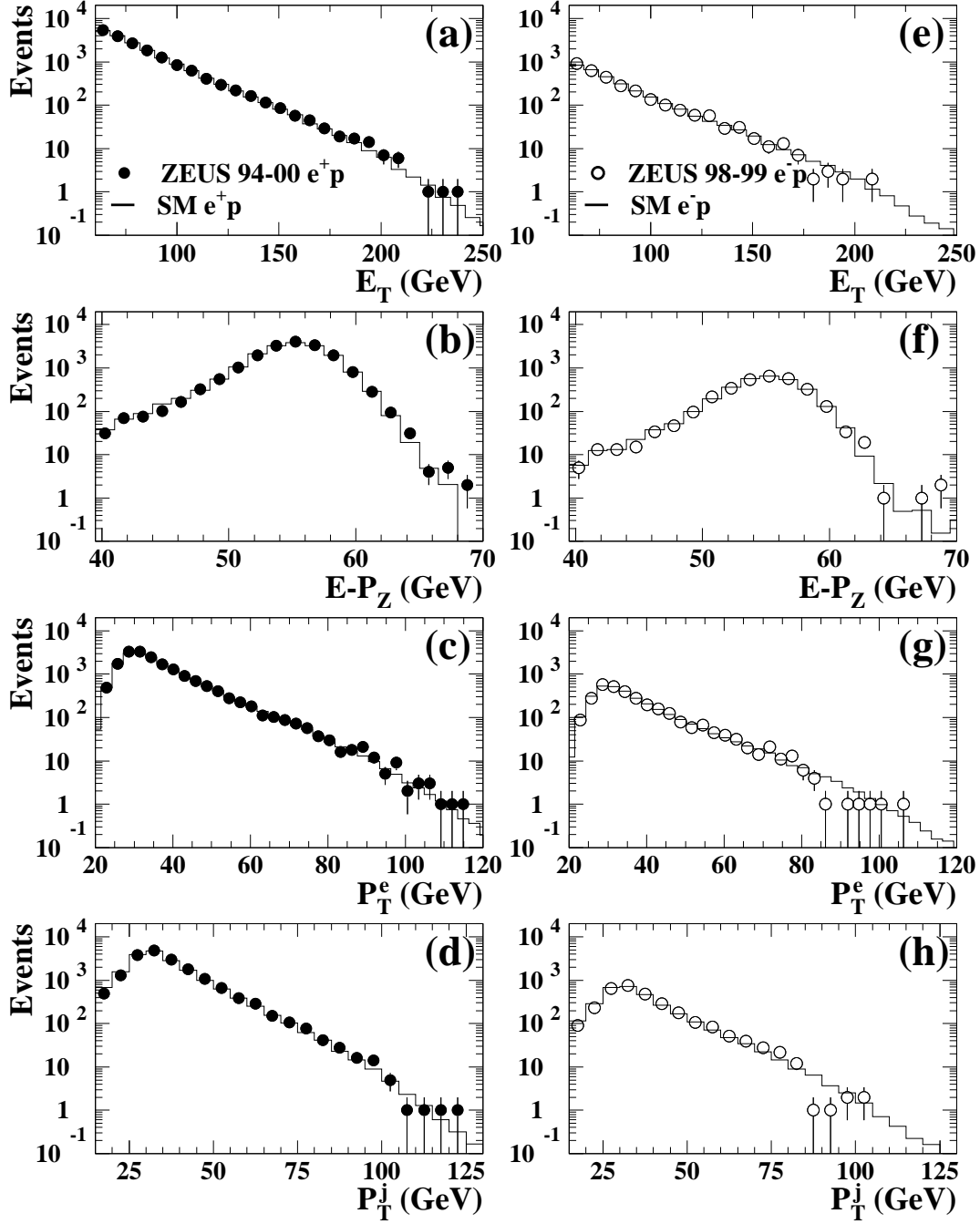


Figure 2: Comparison of distributions from 94-00 e^+p (a-d) and from 98-99 e^-p data sets (e-h) with the corresponding NC MC samples: (a,e) total transverse energy, E_T ; (b,f) $E - P_Z$; (c,g) electron transverse momentum, P_T^e , and (d,h) jet transverse momentum, P_T^j .

ZEUS

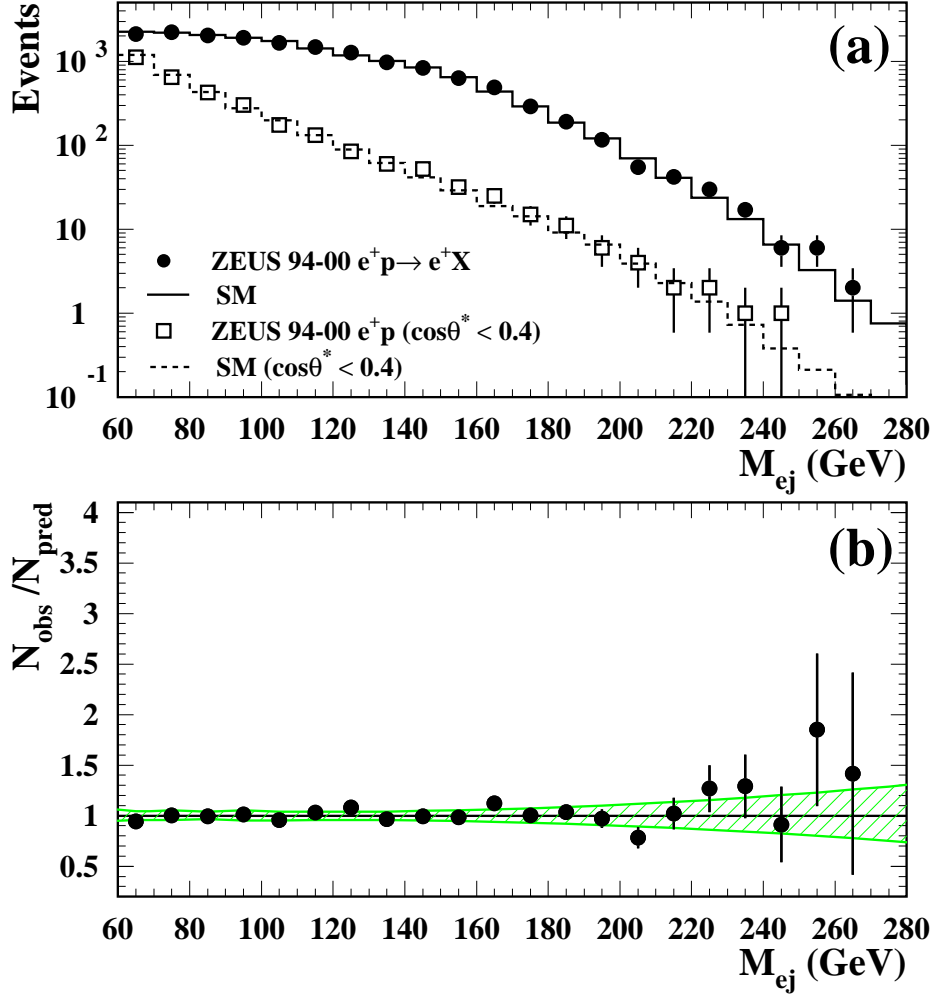


Figure 3: (a) Comparison of the e^+p samples (dots) and the NC SM expectations (solid histogram) for the reconstructed invariant mass M_{ej} in the $e^+p \rightarrow e^+X$ topology. The data (open squares) and the SM expectations (dashed histogram) after the $\cos\theta^* < 0.4$ cut are also shown. (b) The ratio between the data and the SM expectation before the $\cos\theta^*$ cut. The shaded area shows the overall uncertainties of the SM MC expectation.

ZEUS

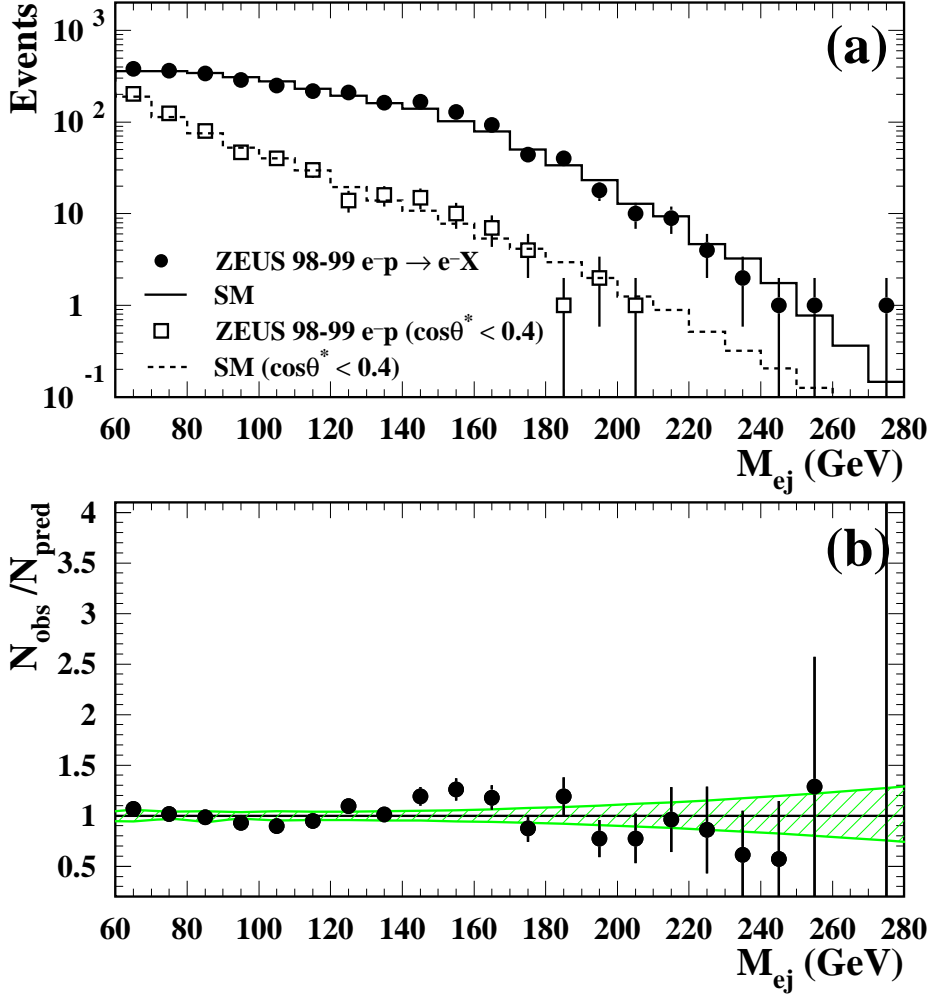


Figure 4: (a) Comparison of the observed e^-p samples (dots) and the NC SM expectations (solid histogram) for the reconstructed invariant mass M_{ej} in the $e^-p \rightarrow e^-X$ topology. The data (open squares) and the SM expectations (dashed histogram) after the $\cos\theta^* < 0.4$ cut are also shown. (b) The ratio between the data and the SM expectation before the $\cos\theta^*$ cut. The shaded area shows the overall uncertainties on the SM MC expectation.

ZEUS

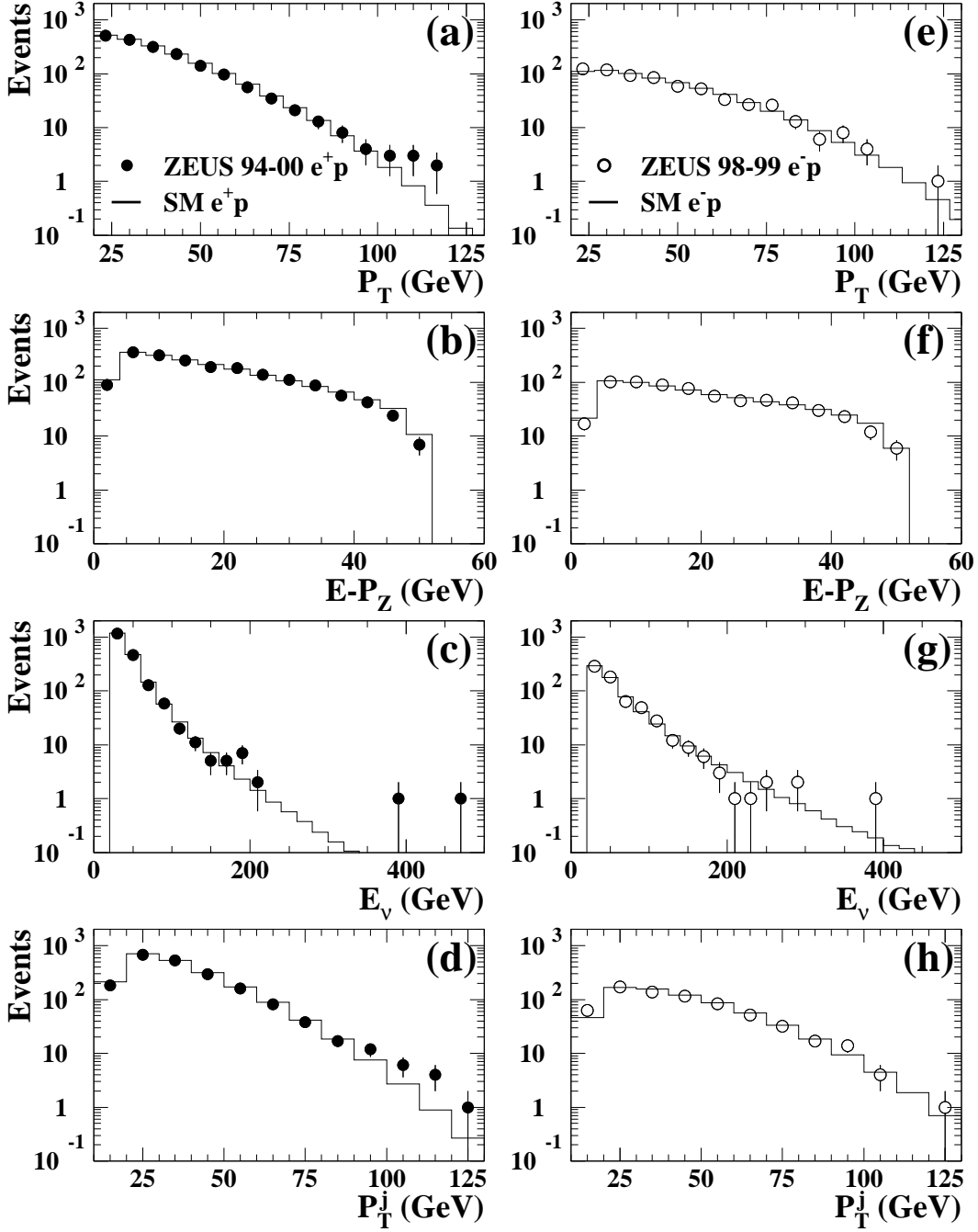


Figure 5: Comparison of distributions from 94-00 e⁺p (a-d) and from 98-99 e⁻p data sets (e-h) with the corresponding CC MC samples for the selected distributions: (a,e) missing transverse energy, P_T ; (b,f) $E - P_Z$; (c,g) neutrino energy, E_ν , and (d,h) jet transverse momentum, P_T^j .

ZEUS

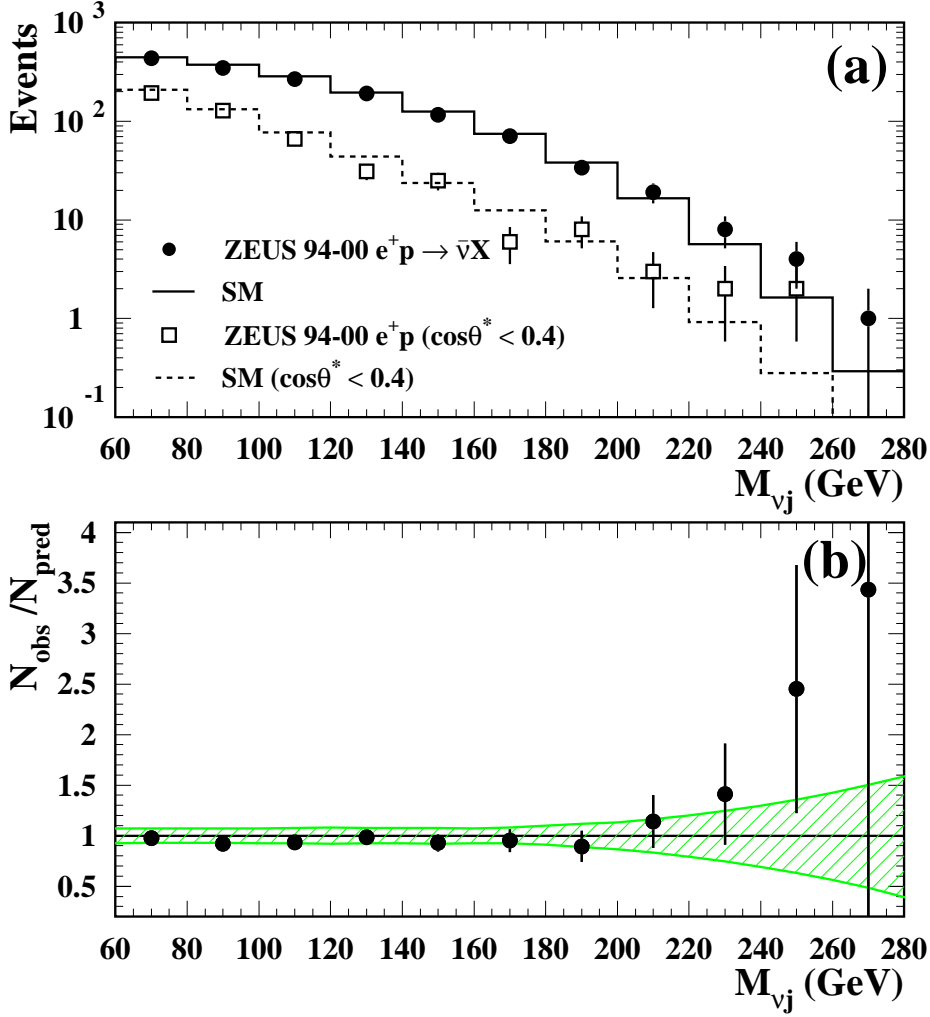


Figure 6: (a) Comparison of the observed e^+p samples (dots) and the CC SM expectations (solid histogram) for the reconstructed invariant mass $M_{\nu j}$ in the $e^+p \rightarrow \bar{\nu}X$ topology. The data (open squares) and the SM expectations (dashed histogram) after the $\cos\theta^* < 0.4$ cut are also shown. (b) The ratio between the data and the SM expectation before the $\cos\theta^*$ cut. The shaded area shows the overall uncertainties on the SM MC expectation.

ZEUS

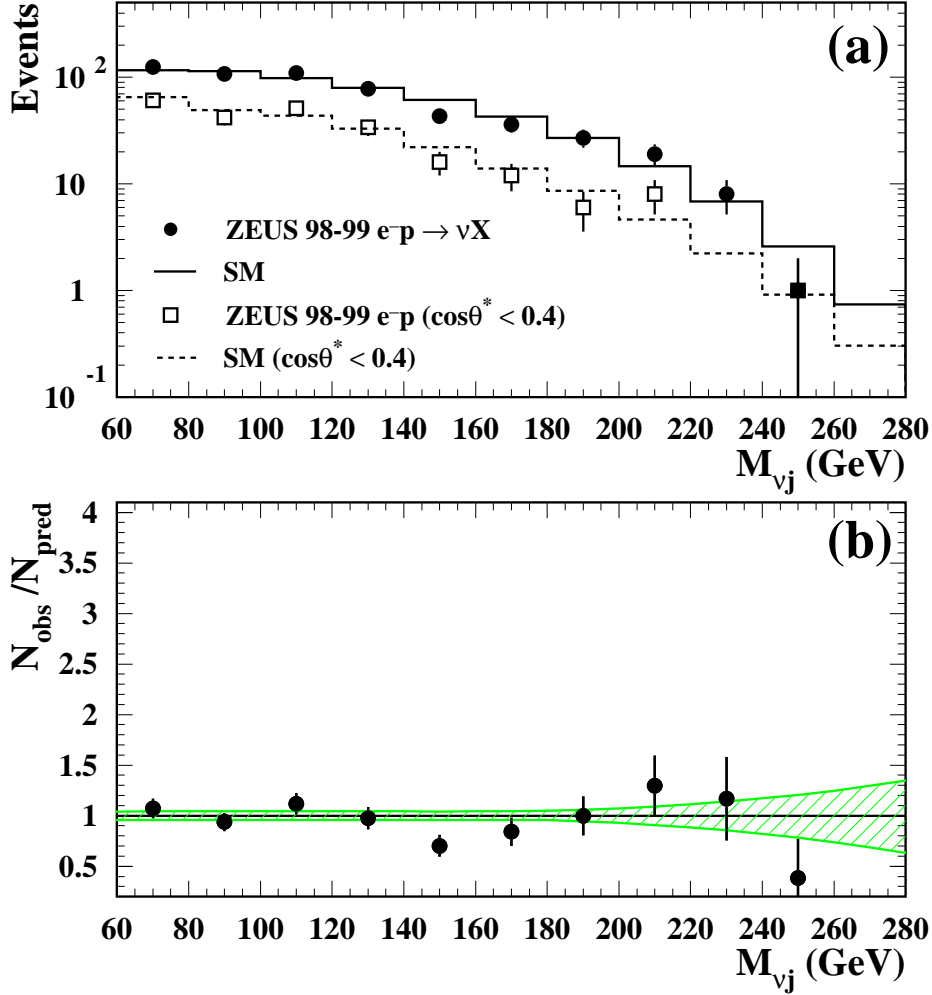


Figure 7: (a) Comparison of the observed e^-p samples (dots) and the CC SM expectations (solid histogram) for the reconstructed invariant mass $M_{\nu j}$ in the $e^-p \rightarrow \nu X$ topology. The data (open squares) and the SM expectations (dashed histogram) after the $\cos\theta^* < 0.4$ cut are also shown. (b) The ratio between the data and the SM expectation before the $\cos\theta^*$ cut. The shaded area shows the overall uncertainties on the SM MC expectation.

ZEUS

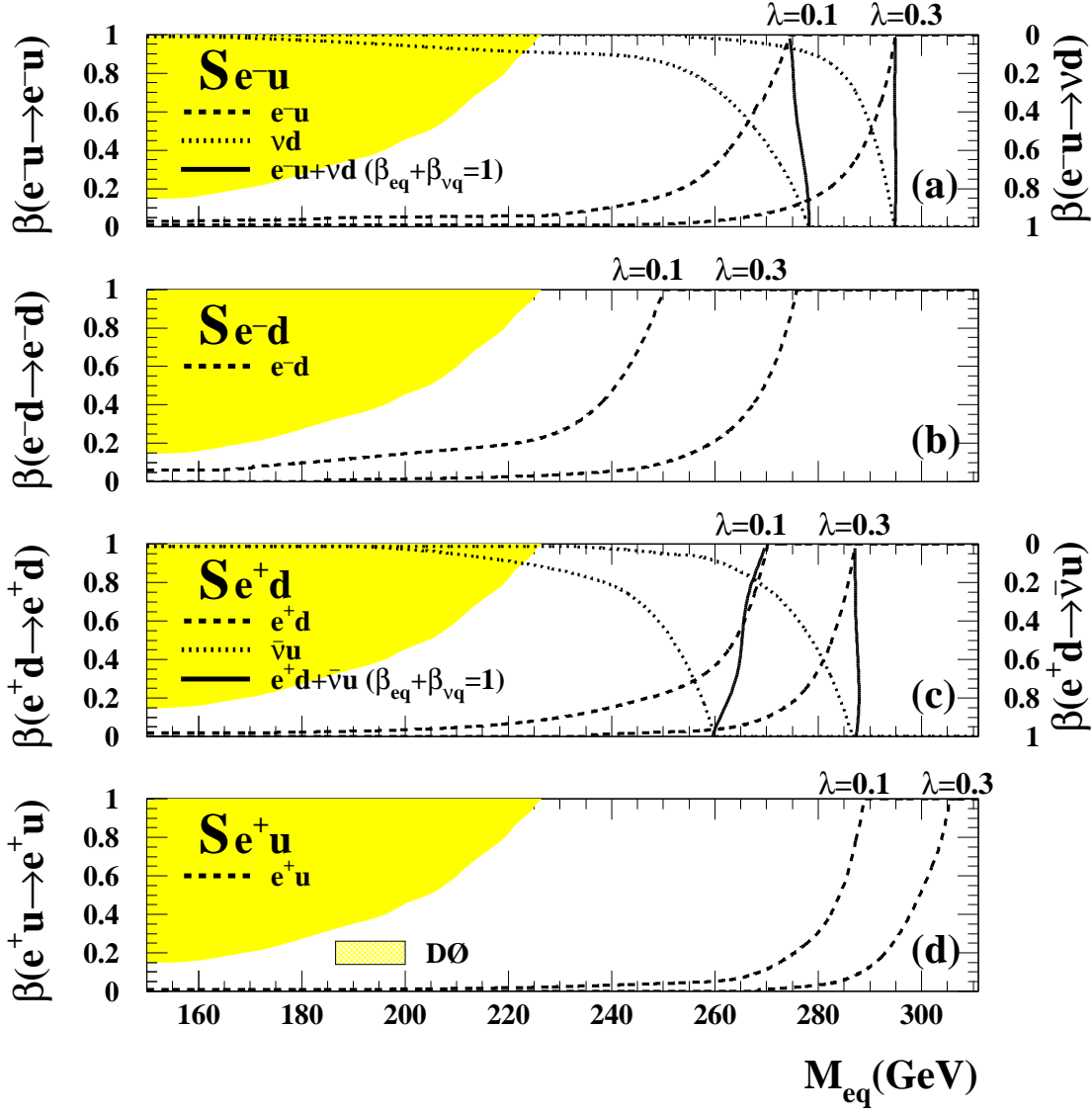


Figure 8: The constant- λ limits as a function of the branching ratios into $e q$ and νq (shown on the left and right axes, respectively), and of the resonance mass (x axes), for the scalar resonant states listed in Table 4. The dotted line corresponds to limits set with only the $e p \rightarrow \nu X$ data set, the dashed line with only the $e p \rightarrow e X$ data set; the solid black line is the limit set using both data sets, assuming $\beta_{eq} + \beta_{\nu q} = 1$. For each limit curve, the area to the left of the curve is the excluded region. Results for the resonant states are shown for constant limit of $\lambda = 0.1$ and $\lambda = 0.3$. The shaded area in each plot shows the area excluded by the $D\bar{0}$ experiment.

ZEUS

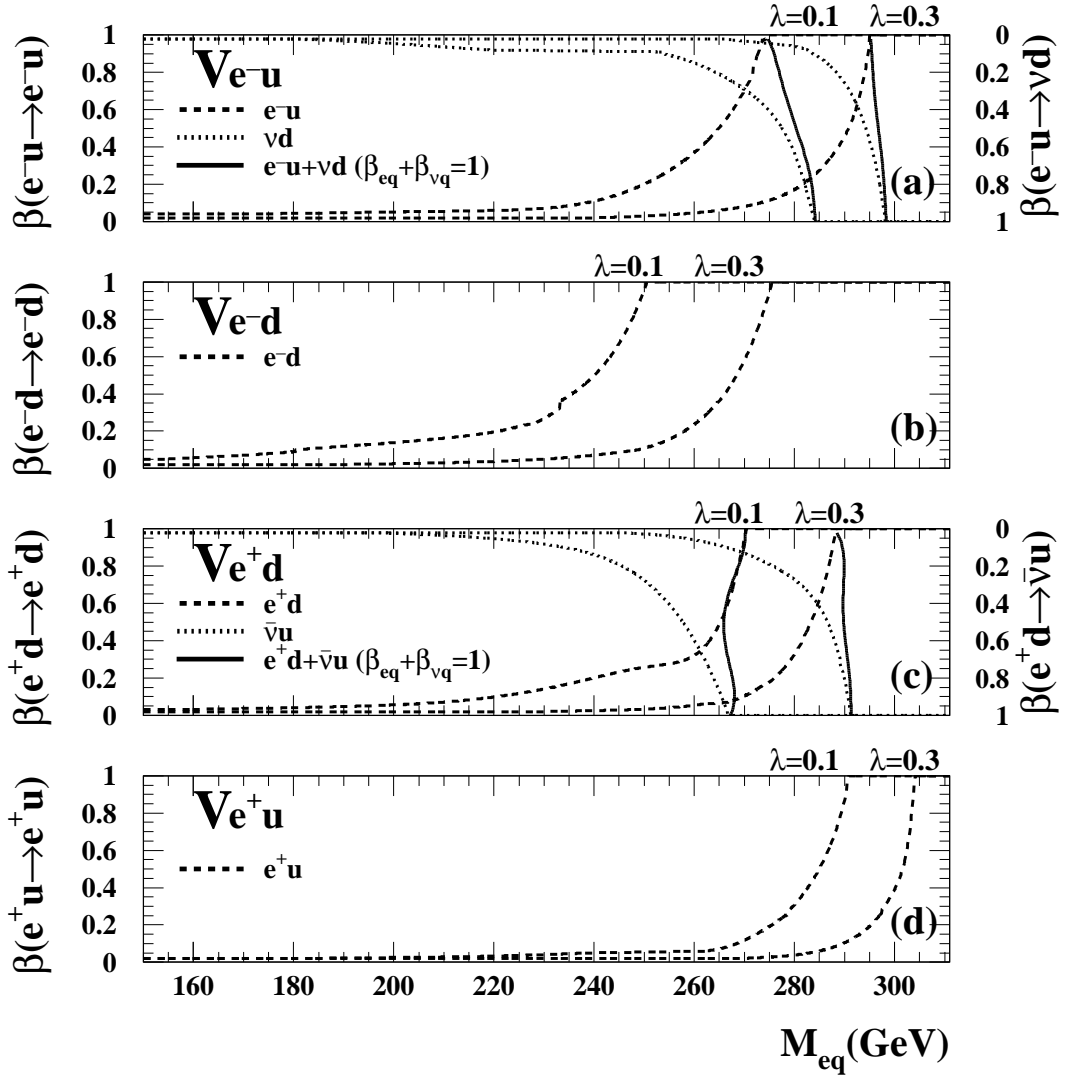


Figure 9: The constant- λ limit contour for the vector resonant states listed in Table 4. For details, see the caption to Fig. 8.

ZEUS

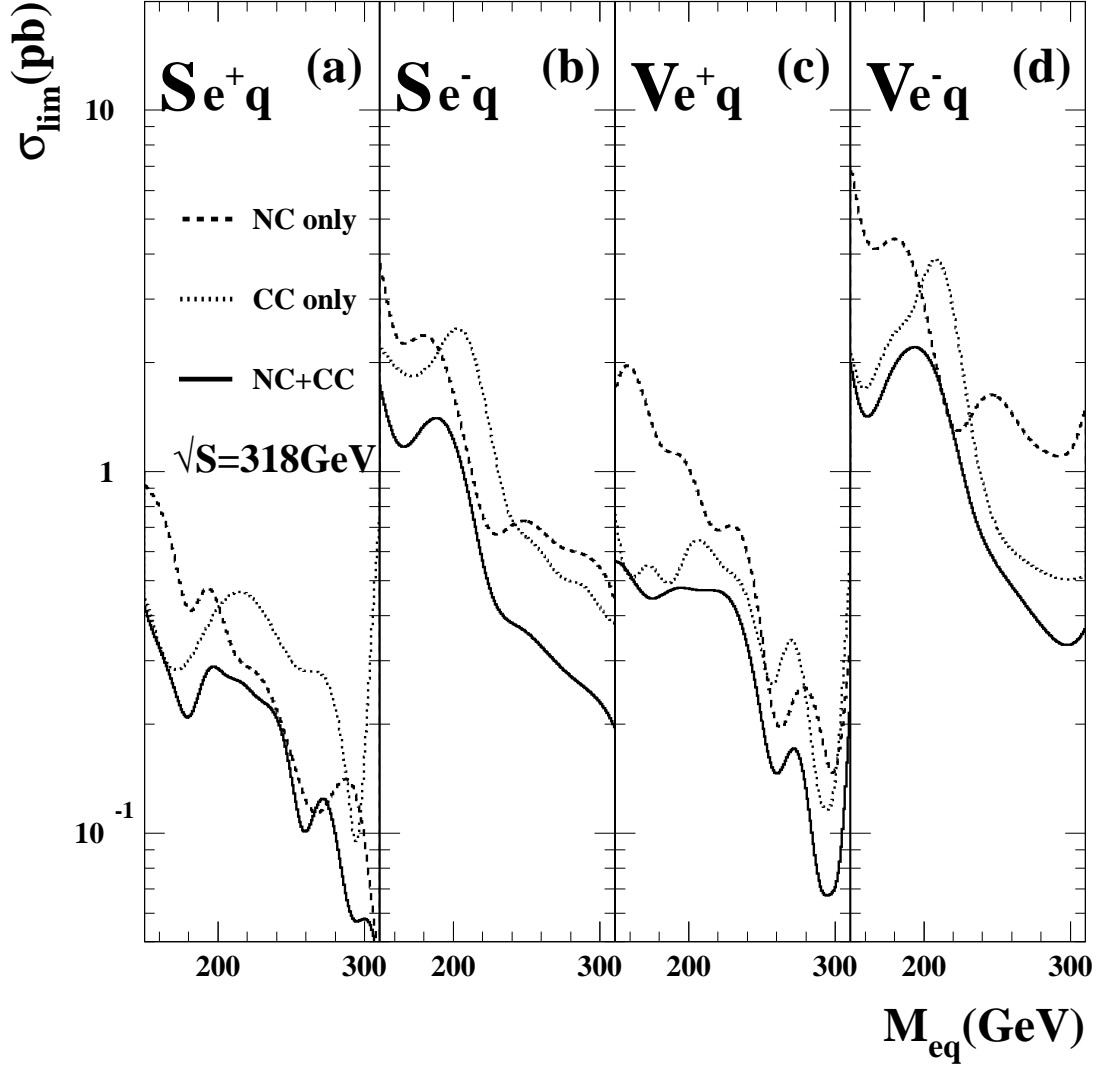


Figure 10: (a,b) Limits on the total production cross section for a narrow scalar resonant state and (c,d) the corresponding limits for a narrow vector resonant state as shown in Table 4. Limits derived from NC (CC) data samples assume a branching ratio β_{eq} ($\beta_{\nu q}$) of 1/2, while the combined $eq + \nu q$ limits assume branching ratios of $\beta_{eq} = \beta_{\nu q} = 1/2$.

ZEUS

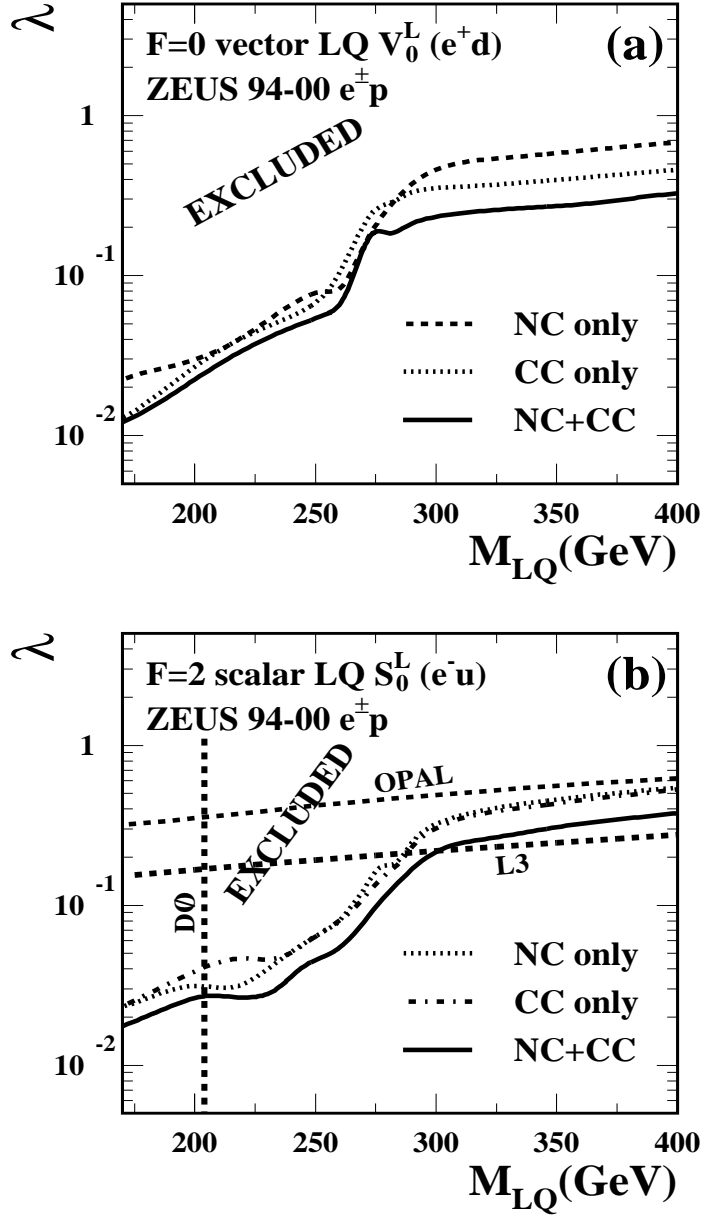


Figure 11: Coupling limits as a function of LQ mass for (a) $F=0$ BRW LQ V_0^L and for (b) $F=2$ BRW LQ S_0^L .

ZEUS

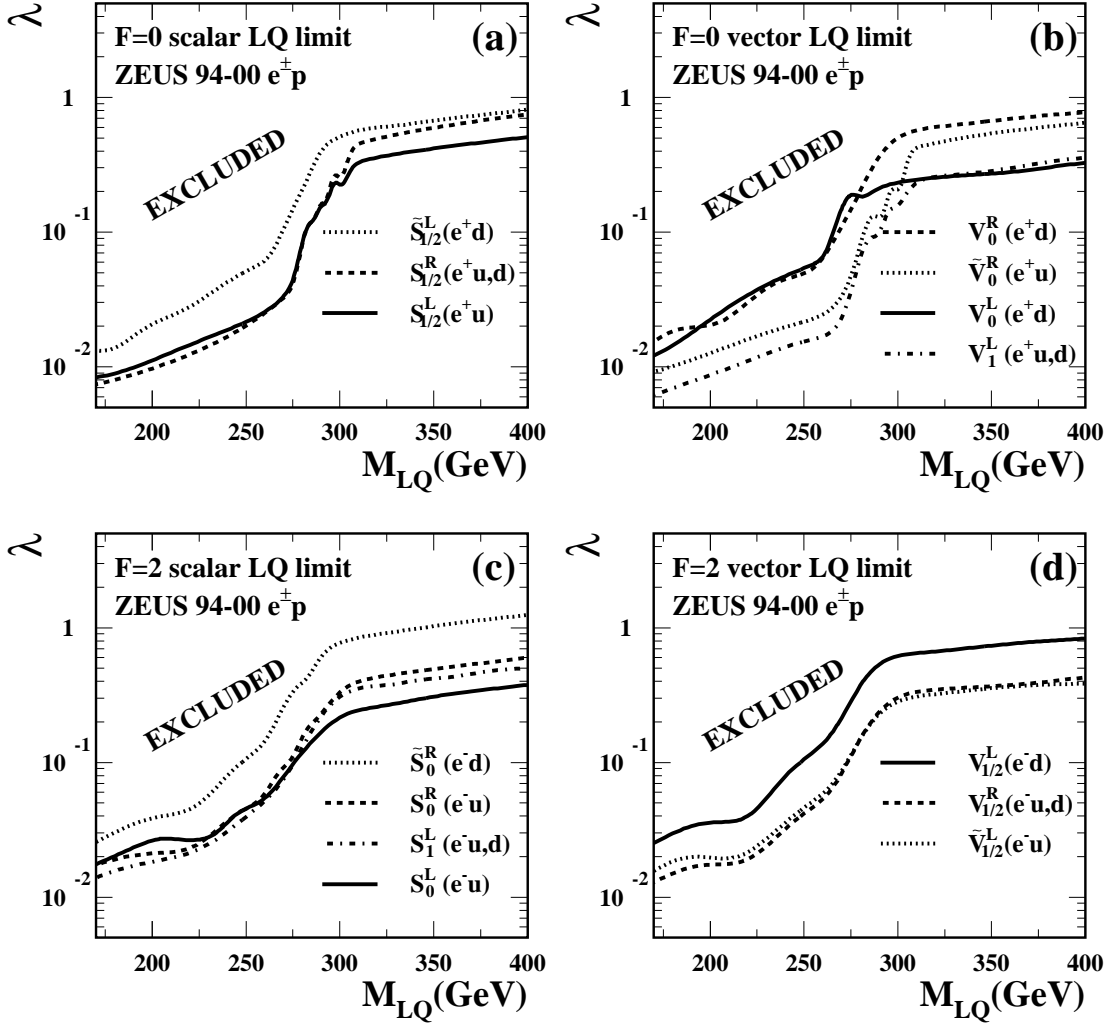


Figure 12: Coupling limits as a function of LQ mass for scalar (a) and vector (b) $F=0$ BRW LQs and for scalar (c) and vector (d) $F=2$ BRW LQs. The areas above the curves are excluded.